

Dynamics of gas-liquid interfaces in turbulent flows over superhydrophobic surfaces

By R. García-Mayoral[†], J. Seo AND A. Mani

The present work studies superhydrophobic surfaces for turbulent drag reduction, focusing on the effect of finite surface tension for the interfaces between the overlying water flow and the pockets of gas attached to the surface. It has been previously reported (Seo *et al.* 2013a) that, once the interface is not assumed to be perfectly rigid, spanwise-coherent, upstream-traveling waves can develop, increasing the pressure fluctuations that the interfaces experience. Here we study the nature and scaling of those waves through direct numerical simulation and quasi-analytical modeling. The results suggest that the waves are not directly connected to the overlying turbulence or the lengthscale of the roughness protrusions, but to the capillary waves that develop from the normal modes of oscillation of the interface as a membrane.

1. Introduction

The reduction of skin friction in turbulent flows has been an active area of research for several decades, and different strategies have been proposed and studied with mixed success. Of these, superhydrophobic surfaces have received a great deal of attention recently for naval applications. Superhydrophobicity enables textured surfaces immersed in water to entrap pockets (or bubbles) of air. The bubbles can lodge within the texture grooves, when the groove size is small enough. This is known as the Cassie-Baxter state. In the opposite, fully wetted condition, or Wenzel state (Wenzel 1936), the surface cavities are filled with water, and the hydrophobic effect is lost. Under Cassie-Baxter conditions, much of the overlying water flow is in contact with the entrapped air, instead of with the solid surface. The air layer acts then as a lubricant for the outer flow, which can effectively slip over the wall, experiencing reduced friction compared to conventional, smooth surfaces (Rothstein 2010). Ou & Rothstein (2005) showed experimentally that, under turbulent conditions, superhydrophobic surfaces are able to achieve high drag reductions, of up to at least 25%. Min & Kim (2005) studied the reduction for turbulent flows numerically, modeling the superhydrophobicity of the surface as a homogeneous slip length, which implies that the surface texture modeled is isotropic. To account for texture anisotropy, Busse & Sandham (2012) recently proposed different streamwise and spanwise slip lengths, although under these conditions the non-uniformity of the texture is still neglected. The detailed geometry of the texture was first studied in simulations by Martell *et al.* (2009), who used a patterned slip/no-slip boundary condition to model the alternating contact with the entrapped air pockets and the roughness crests.

Although the drag-reducing properties of superhydrophobic surfaces on turbulent flows have received a great deal of attention recently, both experimentally (Ou & Rothstein 2005; Gogte *et al.* 2005; Daniello *et al.* 2009; Park *et al.* 2014) and numerically (Min & Kim 2005; Martell *et al.* 2009, 2010; Park *et al.* 2013; Türk *et al.* 2014; Jelly *et al.* 2014),

[†] Department of Engineering, University of Cambridge, UK

the interaction of these surfaces with the flow is not yet fully understood. Most experimental measurements reported have been conducted at texture sizes of order $L^+ \approx 0.5\text{--}5$, where the $+$ superscript denotes scaling with the kinematic viscosity ν and the friction velocity u_τ . Although no clear reason is given, it is likely that for larger textures the stability of the bubbles is lost, and with it the drag-reducing effect. Otherwise, they would yield larger drag reductions than smaller textures, and be more interesting from an application perspective. In contrast, numerical simulations have often been conducted at $L^+ \approx 10\text{--}200$, frequently towards the upper limit. This is due to a compromise between computational cost and physical fidelity, but it is not clear if some of the dynamics that are dominant in this range of L^+ are also important at the smaller sizes of real applications. Even more, it is questionable whether the air bubbles would even remain attached to the surface at such large L^+ were their stability not forcefully imposed through the assumptions in the numerical model. In particular, the above cited simulations assumed that the gas-liquid interfaces maintained a perfectly flat, rigid shape. The reduction predicted in these numerical studies always increases with L^+ , in agreement with the theoretical predictions of Lauga & Stone (2003), Fukagata *et al.* (2006), and Ybert *et al.* (2007), although the behavior deviates from theory for large textures. In real flows, however, the superhydrophobic effect would be completely lost for sufficiently large grooves, once the Cassie-Baxter state is lost and the surface fully wetted (Aljallis *et al.* 2013).

Some work has begun to appear on possible degrading effects, which would eventually lead to the depletion of the gas pockets, but the mechanisms that cause the degradation remain largely unknown. Hyv aluoma & Harting (2008) and Teo & Khoo (2010) have studied the effect of bubble shape when the interface is not perfectly flat, while Busse & Sandham (2013) have analyzed how the performance degrades as the air layer is lost, and the texture crests begin to protrude out of it, introducing a roughness-like effect. Lee & Kim (2009), Patankar (2010), and Samaha *et al.* (2011) have analyzed the transition from the Cassie-Baxter to the Wenzel state through static pressure effects, while Aljallis *et al.* (2013) have considered the effect of shear on bubble depletion at high Re.

The research in our group has also focused on possible degrading mechanisms. In Seo *et al.* (2013*b*), we studied the scaling with L^+ of the pressure forces on the gas-liquid interfaces, finding that pressure peaks, caused by the stagnation of the flow in front of the solid protrusions, can increase rapidly with L^+ , leading to the depletion of the gas layer. More importantly, we have pioneered in including the effect of gas-liquid interfacial deformation in fully turbulent simulations (Seo *et al.* 2013*a*). The surface deformation is introduced through a linearized boundary condition, connecting the wall-normal velocity of the interface with the local pressure fluctuations through a Young-Laplace equation. In Seo *et al.* (2013*a*), we reported the appearance of spanwise-coherent traveling waves, which generate additional large pressure fluctuations on the interface. These waves are qualitatively different from the Kelvin-Helmholtz structures reported over other drag-reducing textured surfaces (Garc a-Mayoral & Jim enez 2011, 2012), as they travel upstream.

The present work focuses on these novel upstream-traveling structures, and explores their scaling with the different dimensionless parameters that account for the interface capillarity and the effect of turbulence. The paper is organized as follows. In Section 2 we present the equations for the problem, discuss the key dimensions and dimensionless parameters, and outline the numerical method used. The results of our simulations are presented and discussed in Section 3. A quasi-analytical model for the traveling waves is proposed in Section 4, and conclusions are summarized in Section 5.

2. Problem formulation

We consider the motion of a turbulent liquid flow in a channel with superhydrophobic rough walls that have entrapped gas pockets, with the roughness consisting of a doubly periodic texture of characteristic size L . The turbulent liquid flow is governed by the incompressible Navier–Stokes equations, with density $\rho = 1$ and kinematic viscosity ν .

The flow is bounded by the protruding roughness elements and the gas pockets interspersed between them. No-slip is imposed at the solid-liquid interfaces, and free shear at the gas-liquid ones. All the boundaries are impermeable, but, while the solid-liquid ones are considered to be rigid, the gas-liquid ones deform in response to the local instantaneous pressure jump across, $p_{gas} - p_{liquid}$, following a Young-Laplace equation,

$$\nabla^2 \eta \approx \frac{p_{liquid} - p_{gas}}{\sigma}, \quad (2.1)$$

where σ is the surface tension and η the interface height. The rough elements are assumed to have flat crests with infinitely sharp edges, so that the gas-liquid interface is effectively pinned to those edges. We neglect the dynamics of the gas within the pockets, assuming that p_{gas} is uniform and that the mass of gas is globally preserved.

Under these conditions, the dimensional analysis of the problem produces a series of dimensionless parameters. The first is a Reynolds number based on the channel half-height, for instance the friction Reynolds number $Re_\tau = u_\tau \delta / \nu$, which measures how turbulent the flow is. For realistic naval applications, with a moving body of meter-scale length and a velocity of order ~ 5 m/s, Re_τ is typically ~ 4000 , a value barely reachable by direct numerical simulation at present. As a compromise, we run our simulations at $Re_\tau \approx 200$ – 400 . Given that the effect of our near-wall manipulations does not extend beyond ~ 40 – $50\nu/u_\tau$, these values are, in principle, high enough to represent the near-wall flow correctly (García-Mayoral & Jiménez 2012). Another important Reynolds number is the size of the texture in viscous units $L^+ = u_\tau L / \nu$, which measures how much the flow deviates from a canonical, smooth-wall flow. Typical experimental values are $L^+ \approx 2$ – 4 , but, because of computational realizability, we have run our simulations at $L^+ \approx 75$ – 150 . Although these values produce unrealistically large slip velocities and drag reductions, they are comparable to the state-of-the-art simulations with patterned textured surfaces (Türk *et al.* 2014; Jelly *et al.* 2014). Nevertheless, the discrepancy with realistic L^+ values has to be taken into account when analyzing the results. The last key dimensionless number is the Weber number, which measures the relative importance of the surface tension. Using inner scaling, the Weber number can be defined as $We^+ = \rho u_\tau \nu / \sigma$. We^+ is appropriate to dimension variations of the interface height η caused by the turbulent pressure fluctuations, which have a wall-parallel lengthscale of order $\sim 100\nu/u_\tau$. On the other hand, if the surface texture size L is smaller than $\sim 100\nu/u_\tau$, the lengthscale of fluctuations of η is constrained by L . In this limit, a more suitable dimensionless number is $We_L = \rho u_\tau^2 L / \sigma$. This scaling has been thoroughly discussed in Seo *et al.* (2013*b*). In the present simulations, with $L^+ \sim 100$, both scalings result in Weber numbers of the same order. However, for smaller textures, the relative importance of capillarity is determined by We_L alone, as the interfaces become relatively stiffer. Since we are interested in reproducing the deformability of the interfaces for empirically realizable values L^+ , we select the value of σ so that We_L matches that of smaller textures, typically $We_L = 2 \times 10^{-3}$. This implies that the interfaces in our simulations have a deformability comparable to those of real air-water interfaces for textures with $L^+ \sim 5$. For $L^+ \sim 150$, real interfaces would be much more flexible.

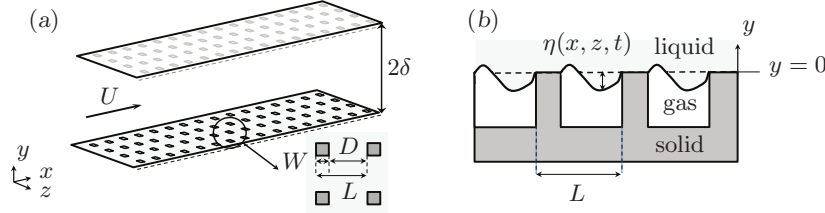


FIGURE 1. (a) Schematic representation of a channel with superhydrophobic-surface boundary conditions on both walls, formed by an array of squared-section solid posts, and the free-slip gas interfaces interspersed between them. W is the post width, D the distance between posts, and $L = W + D$ the total size of the pattern. (b) Sketch illustrating the deformation of the gas-liquid interface, η .

The problem has been numerically solved using the algorithm described in Seo *et al.* (2013b), which we briefly outline here. We use a second-order finite-difference scheme on a staggered mesh. The grid is Cartesian, uniform in the streamwise (x) and spanwise (z) directions, and with stretching in the wall-normal (y) direction. The computational domain is a periodic channel of length $L_x = 2\pi$, width $L_z = \pi$ and height $L_y = 2$. The grid resolution in the wall-normal direction is $\Delta y_{\min}^+ \approx 0.15$, $\Delta y_{\max}^+ \approx 12$. In the streamwise and spanwise directions, the resolution is sufficient both to fully resolve the turbulent eddies, $\Delta x^+ \approx 6.4$, $\Delta z^+ \approx 3.2$, and the smaller-scale flow induced by the surface texture, $\Delta x = \Delta z = L/24$. The time discretization is Crank-Nicholson for the wall-normal viscous terms and Adams-Bashforth for the rest, with a fractional step implementation. The flow is driven by a time-constant mean pressure gradient. The gas-liquid interface is modeled as a perfect-slip boundary condition, resulting in a pattern of slip and no-slip conditions. We study patterns like the one sketched in Figure 1(a), made up of posts distributed uniformly along x and z . We run simulations with post spacings $L^+ \approx 78$ and 155. The post thickness is set to $W = L/3$, resulting in a solid fraction of $1/9$. To consider the effect of the deformation of the gas-liquid interface in response to the overlying pressure fluctuations, we define η as the interface height, measured from the plane that contains the no-slip, flat top of the posts, $y^+ = 0$, as sketched in Figure 1(b). We assume that η is small, and model its fluctuations through a linearized boundary condition for the wall-normal velocity at $y^+ = 0$. Over the solid posts, η is assumed to be zero, while over the gas pockets it is allowed to fluctuate in response to the pressure jump across the interface, according to Eq. (2.1), assuming that p_{gas} is uniform. The motion of the interface generates a non-zero wall-normal velocity at the interface, which is connected to the deformation through its material derivative, $v_{y=0} = \partial_t \eta + u \partial_x \eta + w \partial_z \eta$. The coupling between pressure, interface location, and velocity is resolved explicitly. The simulations have been run for at least $35\delta/u_\tau$, where δ/u_τ is the characteristic turnover time for the largest eddies. The first $10\delta/u_\tau$ interval is left out for statistical sampling, to avoid contamination by initial transients.

3. Simulation results

In Seo *et al.* (2013a), we showed for the first time the effect of interfacial deformation in a fully turbulent flow, by comparison with an equivalent simulation with perfectly flat interfaces. The original setup had $Re_\tau = 395$, $L^+ = 155$ and $We_L = 2 \times 10^{-3}$. We present here a new set of simulations with those parameters modified independently, so their influence can be studied separately. The parameters for each simulation are given in Table 1. Because of time and computational limitations, only four simulations have been

Case	L^+	Re_τ	We_L	n_x	n_z	N_y
S78	77.56	197.5	1×10^{-3}	24	24	128
S78W	77.56	197.5	2×10^{-3}	24	24	128
S155	155.1	197.5	2×10^{-3}	24	48	128
L155	155.1	395.0	2×10^{-3}	24	48	192

TABLE 1. Simulation parameters. L^+ is the texture pattern spacing in wall units, Re_τ is the friction Reynolds number, and $\text{We}_L = \rho u_\tau^2 L / \sigma$ is the Weber number. The spatial resolution is given by n_x and n_z , the number of streamwise and spanwise points per pattern unit, and N_y , the number of points in the wall-normal direction.

conducted. From the benchmark case S155, the other three simulations have different Re_τ , L^+ or We_L . A more thorough exploration of the parametric space is left for future studies. Simulation L155 is very similar to that of Seo *et al.* (2013a), except for a slightly increased solid fraction, to reduce the resolution required to capture the flow near the solid posts. The benchmark case, S155, differs from L155 only in Re_τ , which was set to $\text{Re}_\tau = 197.5$ to scale down the simulation cost for this and the remaining cases. From case S155, L^+ was halved for cases S78 and S78W. For S78, the surface tension σ is kept constant, instead of the dimensionless We_L . In a laboratory experiment, the equivalent would be to reduce L while maintaining the same gas and liquid species. In turn, case S78W keeps We_L constant, which would be equivalent to changing L and σ by the same factor. This would require changing the gas and liquid species for the experiment, to obtain a more wobbly interface.

The upstream-traveling, spanwise-coherent structures reported in Seo *et al.* (2013a) can be once more observed in our present simulations. However, their appearance is clear only for the larger textures of cases L155 and S155. For S78 and S78W, their coherence is apparently lost, even if there are still structures traveling in the upstream direction. The corresponding pressure signals at a given instant are portrayed in Figure 2. The figure also shows the stationary stagnation regions in front of the posts, which were discussed elsewhere (Seo *et al.* 2013b), but the presence of the spanwise-coherent waves is clearly visible for the simulations with $L^+ = 155$. For $L^+ = 78$, the structures are weaker, and their presence is obscured by the superimposed turbulent fluctuations.

A more quantitative representation of these waves can be obtained through the space-time correlation of the signal. The correlations for the four cases are portrayed in Figure 3, where the coherence of the waves is clear, both in space and time. The correlations show distinctively two separate motions at the interface, the conventional advection of near-wall turbulence and the coherent upstream-traveling waves. The advection of turbulence occurs for smooth no-slip walls at $U_{a,\text{smooth}}^+ \approx 10$. Over our slipping surfaces, where there is an additional slip velocity $U_s^+ \approx 15$ for $L^+ \approx 78$ and $U_s^+ \approx 21$ for $L^+ \approx 155$, the advection is closer to $U_a^+ \approx U_{a,\text{smooth}}^+ + U_s^+$, as shown in the figure.

The footprints of the upstream-traveling waves are even clearer. For cases S155 and L155, the waves are essentially the same, suggesting that they have little dependence on Re_τ , and justifying the validity of simulations at low Reynolds numbers, provided the rest of parameters are scaled in wall units. For the two cases at $L^+ \approx 155$, the streamwise wavelength is $\lambda_x^+ \approx 320$, and the phase velocity is $U_c^+ \approx -35$. The wavelength and velocity of the waves change for the two cases at smaller L^+ . Although further studies are required to clarify the scaling, covering the parameter space more extensively, a first

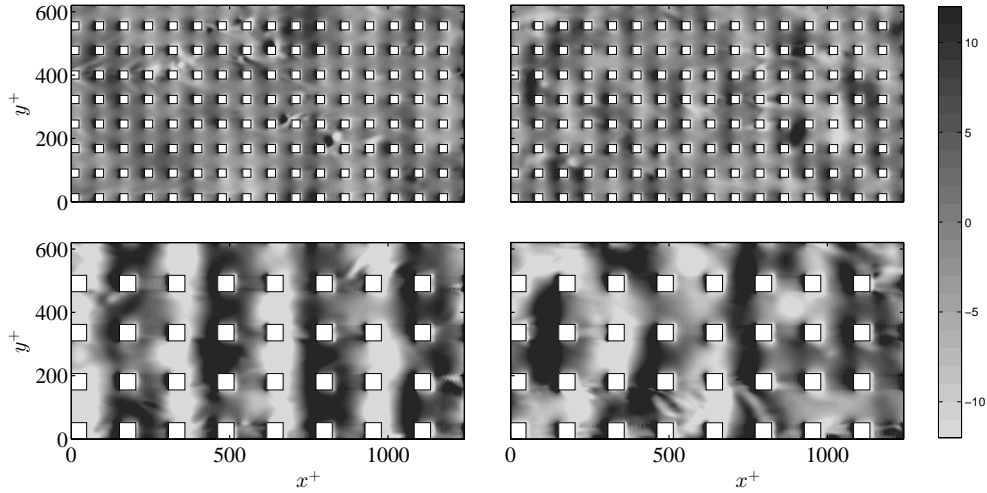


FIGURE 2. Comparison of instantaneous pressure fluctuations p^+ at $y^+ = 0$. From left to right and top to bottom, cases S78, S78W, S155, L155. Note that, for the latter case, only one fourth of the plane $y^+ = 0$ is shown.

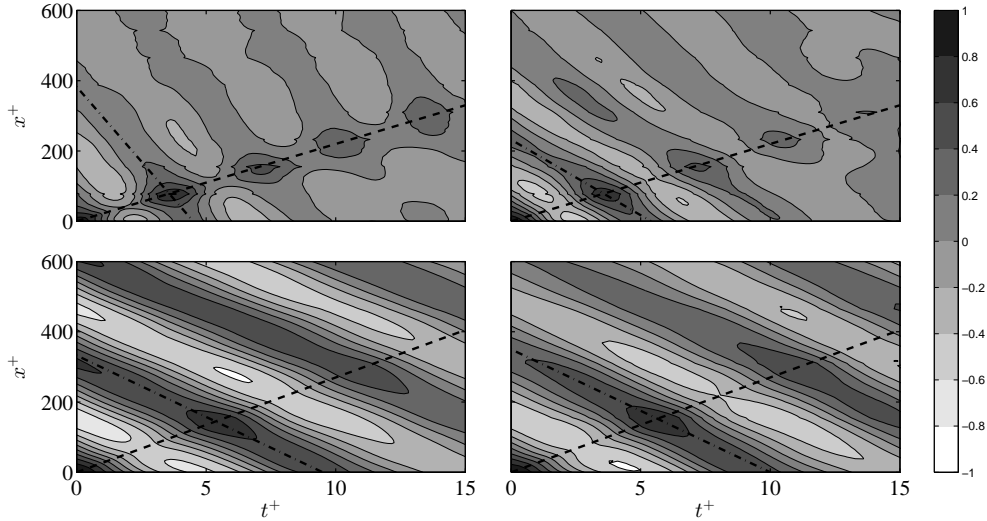


FIGURE 3. Space-time correlation of the pressure signal at $y^+ = 0$. From left to right and top to bottom, cases S78, S78W, S155, L155. The dashed lines represent the mean advection of the turbulent eddies, $U_a^+ \approx 22$ for $L^+ = 78$ and $U_a^+ \approx 28$ for $L^+ = 155$. The dashed-dotted lines represent the phase velocity of the upstream-traveling, spanwise-coherent structures, $U_c^+ \approx -85$ for case S78, $U_c^+ \approx -43$ for case S78W, and $U_c^+ \approx -35$ for cases S155 and L155.

rough analysis suggests that U_c^+ depends mainly on We_L , so that it is essentially the same for cases L155, S155 and S78W, and is roughly doubled when We_L is halved for case S78. The scaling of the streamwise wavelength λ_x^+ is somewhat less clear, but from cases L155 and S155 to S78 there appears to be only a small change, suggesting that λ_x^+ does not scale with L^+ , but instead that $We_\lambda = \rho u_\tau^2 \lambda_x / \sigma$ remains essentially constant. In turn, as σ is halved from case S78 to case S78W, the resulting λ_x is also reduced by almost a factor of two, so that $We_\lambda \approx 5 \times 10^{-3}$ remains again roughly constant. If we define $\sigma^+ = \sigma / \rho v u_\tau$, the wavelength for all four cases roughly follows $\lambda_x^+ \approx 5 \times 10^{-3} \sigma^+$.

The above discussion suggests that, even if the upstream-traveling waves are triggered

and modulated by the presence of the posts, their scaling may be essentially independent of the lengthscale of the post layout. This would be consistent with the characterization of the waves as essentially capillary, similar to conventional capillary waves over smooth, unobstructed gas-liquid interfaces.

4. A quasi-analytical model for the interfacial traveling waves

To study the natural modes of the interface as a flexible, free-slip surface, we propose the following model. Let us consider an inviscid flow of density $\rho = 1$ slipping over a superhydrophobic surface with posts separated a distance $L = 1$, with uniform mean velocity profile $U = 1$, and with small fluctuations $(u, v, w; p)$ about that mean flow. This problem is analogous to that of wave propagation in liquid films (Squire 1953; Taylor 1959), except for the presence of the solid posts, which make the film discontinuous. The fluctuating velocity field can be described in terms of a potential $\psi(x, y, z)$, which satisfies $\nabla^2 \psi = 0$. Using Fourier decomposition along the wall-parallel directions, x and z , the above Poisson equation adopts the form $(-k_x^2 - k_z^2 + \partial_y^2) \hat{\psi} = 0$ for each (k_x, k_z) mode. For vanishing $\hat{\psi}$ at $y \rightarrow \infty$, the solution is $\hat{\psi}(y) = \hat{\psi}_{y=0} \exp(-\sqrt{k_x^2 + k_z^2} y)$. This allows us to write a relationship at $y = 0$ between the potential and its y -derivative,

$$(\partial_y \psi)_{y=0} = F^{-1} K F \psi_{y=0}, \quad (4.1)$$

where F and F^{-1} denote discrete direct and inverse Fourier transform operators, and K is the diagonal matrix formed by the derivative eigenvalues $-\sqrt{k_x^2 + k_z^2}$. Note that, by the definition of the potential, $\partial_y \psi = v$. Therefore, we are interested only in the restriction of Eq. (4.1) that also satisfies $(\partial_y \psi)_{y=0} = v_{y=0} = 0$ over the solid posts.

The potential ψ can also be related to the fluctuating pressure through the linearized inviscid momentum equation,

$$(\partial_t + U \partial_x) \psi = -\frac{1}{\rho} p, \quad (4.2)$$

which can be particularized at $y = 0$. The fluctuating deformation of the interface,

$$(\partial_x^2 + \partial_z^2) \eta = \frac{1}{\sigma} p, \quad (4.3)$$

is connected to the wall-normal velocity through the material derivative,

$$(\partial_t + U \partial_x) \eta = (\partial_y \psi)_{y=0}. \quad (4.4)$$

We are interested in wave solutions for the system of Eqs. (4.1)-(4.4). Using the corresponding transformation $\partial_t = i\omega$, the problem can be written in the frequency- ω domain,

$$A(\omega) \psi_{y=0} = 0, \quad (4.5)$$

where the dependence of A on ω is quadratic. The problem then reduces to finding values of ω for which Eq. (4.5) has a null subspace, and the eigen-solutions in that subspace.

To solve the problem numerically, we have used second-order, centered finite differences on a uniform grid to discretize Eqs. (4.2)-(4.4), with $\Delta x = L/32$ and $\Delta z = L/24$. Solutions exist only for a discrete set of frequencies, and take the form of either upstream- or downstream-traveling waves, with a phase velocity U_c several times larger than the flow velocity U . The first solution, that of smaller ω , is always an upstream-traveling wave, periodic in x and with its wavelength λ_x spanning the full domain considered. To

Reference DNS	U^+	$\tilde{\sigma}$	λ_x/L	$\omega U/L$	$U_{c,model}^+$	$U_{c,DNS}^+$
S78	15	4.45	6	7.3943	-105.9155	-85
S78	22	2.05	6	4.6555	-97.8049	-85
S78W	15	2.20	3	6.9991	-50.1274	-43
S78W	22	1.05	3	4.1680	-43.7816	-43
S155,L155	21	1.15	2	5.8496	-39.1017	-35
S155,L155	28	0.65	2	3.6413	-31.2947	-35

TABLE 2. Solutions to the linearized, inviscid flow over superhydrophobic posts. From each DNS, U for the model is estimated as either the slip or the mean advection velocity, $U^+ = U_s^+$ or $U^+ = U_a^+$, to obtain a surface tension $\tilde{\sigma} = 1/(U^{+2}We_L)$. From all the possible frequencies ω for which Eq. (4.5) is satisfied, only the one with wavelength λ_x/L close to that observed in the DNS is shown. $U_{c,model}^+$ is the phase velocity of the corresponding solution, to be compared with that measured from the DNS, $U_{c,DNS}^+$.

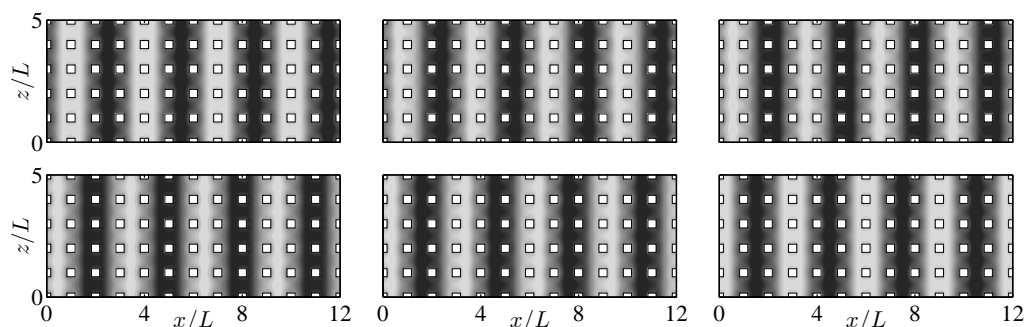


FIGURE 4. Instantaneous realizations of the pressure at $y = 0$ for the model problem with $\tilde{\sigma} = 1.05$ and $\lambda_x/L = 3$. From left to right and top to bottom, $t = 2\pi L/\omega\lambda_x \times [0 : 0.2 : 1]$

capture the solutions observed in our DNSs, with $\lambda_x \approx 5L$ for case S78, $\lambda_x \approx 3L$ for case S78W, and $\lambda_x \approx 2L$ for cases S155 and L155, we have sought solutions for Eq. (4.5) in a domain of length $L_x = 12L$. This length should be sufficiently large to mitigate the effect of the box length on the wavelength of the solutions, at least for wavelengths near those observed in the DNSs. The values of the dimensionless $\tilde{\sigma} = \sigma/\rho U^2 L$ for the model are chosen to match our DNS setups, taking into account that from the DNSs $\tilde{\sigma} = 1/(U^{+2}We_L)$. Given the coarseness of the model, with a uniform profile for U , establishing a corresponding U^+ can be ambiguous. One straightforward choice is to use U_s^+ , but a more sensible choice may be U_a^+ , since this is the velocity at which the turbulent fluctuations are advected on average, and since they are responsible for triggering the waves at the interface. Table 2 compiles solutions for $\tilde{\sigma}$ values estimated using both U_s^+ and U_a^+ , and for values of λ_x/L close to those observed in the DNSs. The solution corresponding to case S78W when using U_a to estimate $\tilde{\sigma}$ is portrayed as an example in Figure 4. The results agree reasonably well with our observations, but we must note that the model is at present not predictive, since the wavelength of the solution needs to be selected *a posteriori* from the DNS results. The uniform velocity profile is unable to provide a lengthscale for the waves, which is then given by the domain considered. Turbulent profiles have a concentration of $\partial^2 U/\partial y^2$ at $y^+ = 7-10$, which has been shown to set the lengthscale for other coherent waves over complex surfaces (García-Mayoral & Jiménez 2011). A similar mechanism may be important in the present case, so considering the non-uniformity of the profile may be essential for the model to become predictive. A more refined version is presently under development and will be presented in the future.

5. Concluding remarks

In the present work, we have studied the effect of air-water interface deformability in turbulent flows over textured superhydrophobic walls with entrapped pockets of air. As the water flow slips over the air pockets, the friction is reduced compared to conventional, smooth walls. The reduction predicted by previous studies increases with the texture size, scaled in wall units. However, very large features will eventually lead to the instability of the entrapped air pockets, and their depletion. To investigate the deleterious effects eventually leading to that depletion, we have studied the effect of the deformability of the air-water interfaces. We had previously reported the appearance of spanwise-coherent, upstream-traveling waves once the interface is allowed to deform. In this study, we have focused on understanding the dynamics of those traveling waves, and particularly how they are influenced by the flow conditions. For that, we have conducted a series of DNSs, systematically varying the friction Reynolds number and the dimensionless roughness spacing and surface tension. The results suggest that the interfacial waves are actually natural capillary waves of the interface, and that their wavelength is essentially independent of that of the surface texture.

Acknowledgments

The authors would like to thank the Office of Naval Research for support of this research under Grant No. 3002451214.

REFERENCES

- ALJALLIS, E., SARSHAR, M. A., DATLA, R., SIKKA, V. & JONE, A. 2013 Experimental study of skin friction drag reduction on superhydrophobic flat plates in high Reynolds number boundary layer flow. *Phys. Fluids* **25**, 025103.
- BUSSE, A. & SANDHAM, N. D. 2012 Influence of an anisotropic slip-length boundary condition on turbulent channel flow. *Phys. Fluids* **24**, 055111.
- BUSSE, A. & SANDHAM, N. D. 2013 Turbulent flow over superhydrophobic surfaces - roughness versus slip. In *14TH European Turbulence Conference*. Lyon, France.
- DANIELLO, R., WATERHOUSE, N. E. & ROTHSTEIN, J. P. 2009 Turbulent drag reduction using superhydrophobic surfaces. *Phys. Fluids* **21**, 085103.
- FUKAGATA, K., KASAGI, N. & KOUMOUTSAKOS, P. 2006 A theoretical prediction of friction drag reduction in turbulent flow by superhydrophobic surfaces. *Phys. Fluids* **18**, 051703.
- GARCÍA-MAYORAL, R. & JIMÉNEZ, J. 2011 Hydrodynamic stability and breakdown of the viscous regime over riblets. *J. Fluid Mech.* **678**, 317–347.
- GARCÍA-MAYORAL, R. & JIMÉNEZ, J. 2012 Scaling of turbulent structures in riblet channels up to $Re_\tau \approx 550$. *Phys. Fluids* **24**, 105101.
- GOGTE, S., VOROBIEFF, P., TRUESDELL, R., MAMMOLI, A., SWOL, F. V., SHAH, P. & BRINKER, C. J. 2005 Effective slip on textured superhydrophobic surfaces. *Phys. Fluids* **17**, 051701.
- HYVÄLUOMA, J. & HARTING, J. 2008 Slip flow over structured surfaces with entrapped microbubbles. *Phys. Rev. Lett.* **100**, 246001.
- JELLY, T. O., JUNG, S. Y. & ZAKI, T. A. 2014 Turbulence and skin friction modification in channel flow with streamwise-aligned superhydrophobic surface texture. *Phys. Fluids* **26**, 095102.

- LAUGA, J. & STONE, H. 2003 Effective slip in pressure-driven Stokes flow. *J. Fluid Mech.* **489**, 55–77.
- LEE, C. & KIM, C.-J. 2009 Maximizing the giant liquid slip on superhydrophobic microstructures by nanostructuring their sidewalls. *Langmuir* **25**, 12812–12818.
- MARTELL, M. B., PEROT, J. B. & ROTHSTEIN, J. P. 2009 Direct numerical simulations of turbulent flows over superhydrophobic surfaces. *J. Fluid Mech.* **620**, 31–41.
- MARTELL, M. B., ROTHSTEIN, J. P. & PEROT, J. B. 2010 An analysis of superhydrophobic turbulent drag reduction mechanisms using direct numerical simulation. *Phys. Fluids* **22**, 065102.
- MIN, T. & KIM, J. 2005 Effects of hydrophobic surface on skin-friction drag. *Phys. Fluids* **16**, L55–L58.
- OU, J. & ROTHSTEIN, J. P. 2005 Direct velocity measurements of the flow past drag-reducing ultrahydrophobic surfaces. *Phys. Fluids* **17**, 13606.
- PARK, H., PARK, H. & KIM, J. 2013 A numerical study of the effects of superhydrophobic surface on skin-friction drag in turbulent channel flow. *Phys. Fluids* **25**, 110815.
- PARK, H., SUN, G. & KIM, C.-J. 2014 Superhydrophobic turbulent drag reduction as a function of surface grating parameters. *J. Fluid Mech.* **747**, 722–734.
- PATANKAR, N. A. 2010 Consolidation of hydrophobic transition criteria by using an approximate energy minimization approach. *Langmuir* **26**, 8941–8945.
- ROTHSTEIN, J. P. 2010 Slip on superhydrophobic surfaces. *Annu. Rev. Fluid Mech.* **42**, 89–109.
- SAMAHA, M. A., VAHEDI, T. H. & EL HAK, M. G. 2011 Modeling drag reduction and meniscus stability of superhydrophobic surface of random roughness. *Phys. Fluids* **23**, 012001.
- SEO, J., GARCÍA-MAYORAL, R. & MANI, A. 2013a Influence of liquid-gas interface dynamics in superhydrophobic surfaces for drag reduction. In *14TH European Turbulence Conference*. Lyon, France.
- SEO, J., GARCÍA-MAYORAL, R. & MANI, A. 2013b Pressure fluctuations in turbulent flows over superhydrophobic surfaces. *Annual Research Briefs*, Center for Turbulence Research, Stanford University, pp. 217–229.
- SQUIRE, H. B. 1953 Investigation of the instability of a moving liquid film. *Brit. J. Appl. Phys.* **4**, 167–169.
- TAYLOR, G. I. 1959 The dynamics of thin sheets of fluid. ii. Waves on fluid sheets. *Proc. R. Soc. A* **253**, 296–312.
- TEO, C. J. & KHOO, B. C. 2010 Flow past superhydrophobic surfaces containing longitudinal grooves: effects of interface curvature. *Microfluidics and Nanofluidics* **9**, 499–511.
- TÜRK, S., DASCHIEL, G., STROH, A., HASEGAWA, Y. & FROHNAPFEL, B. 2014 Turbulent flow over superhydrophobic surfaces with streamwise grooves. *J. Fluid Mech.* **747**, 186–217.
- WENZEL, R. N. 1936 Resistance of solid surfaces to wetting by water. *Ind. Eng. Chem.* **28**, 988–994.
- YBERT, C., BARENTIN, C. & COTTIN-BIZONNE, C. 2007 Achieving large slip with superhydrophobic surfaces: Scaling laws for generic geometries. *Phys. Fluids* **19**, 123601.